This is the Post print version of a Manuscript in Materials Chemistry Frontiers at DOI https://doi.org/10.1039/D3QM00243H

Molecular insights into growth and time evolution of surface states of $CsPbBr_3$ nanoparticles synthesized by scalable room temperature approach

Received 00th January 20xx,
Accepted 00th January 20xx

DOI: 10.1039/x0xx00000x

Mariangela Giancaspro,[a,b] Roberto Grisorio,[c] Gabriele Alò,[a] Nicola Margiotta,[a] Annamaria Panniello,[b] Gian paolo Suranna,[c,d] Nicoletta Depalo,[b] Marinella Striccoli,[b,e] M. Lucia Curri,[a,c,e] Elisabetta Fanizza[a,c,e,*]

Room temperature ligand-assisted reprecipitation syntheses of $CsPbBr_3$ nanoparticles (NPs) in open air condition and non-polar solvent are recently emerging as viable strategies for large-scale production of highly emissive NPs. These procedures encounter some of the relevant requirements for industrial perspectives i.e. high-quality materials, low cost, and synthesis scalability. Here, starting from reported protocols, *ad hoc* mixtures in anhydrous toluene of precursors (Cs_2CO_3 and $PbBr_2$) and surfactants, as oleyl amine, alkylcarboxylic acid, didodecyl dimethyl ammonium bromide, tetraoctylammonium bromide, octyl phosphonic acid and phosphine oxide, are selected. The careful analysis of NPs morphology, emission properties, reactive species in the mixtures and composition of the ligands bound at NP surface or free in the final colloidal solution allows to tackle still open issues, including achievement of NP monodispersity, high NP production yield and to unveil the mechanisms behind changes of the emission properties in time. NP size dispersion is proved to depend not solely on ligands interaction to NP surface, but also on the bromoplumbates species *in situ* generated in the reaction mixture at caesium-precursor solution injection. Purification methods are carefully adjusted so as not to reduce the NP production yield, caused by aggregation phenomena induced by displacement of loosely bound ligands. Meanwhile, the residual species, left in in the reaction mixture due to limited purification, are demonstrated to effectively contribute over time to the fate of the NP properties. Emission is exploited as effective macroscopic evidence of the NPs molecular and structural modifications. In fact, the emission properties, which could be, in principle, predicted on the basis of the ligand density and binding energy, on long time scales are found to evolve in time due to reaction of the residual molecules with the adsorbed ligands.

Introduction

During the last decades, colloidal all-inorganic lead halide perovskites (LHP) nanoparticles (NPs) have gained enormous interest, due to the plethora of their optical properties, including high absorption coefficient in the visible range, efficient photoluminescence with a narrow emission line widths and defect tolerant behaviour, advantageous for application in optoelectronic and photovoltaic devices.[1-7] The interest towards the technological application of this class of materials, driven by their unique characteristics, currently urges the quest of large-scale production methods, aiming at filling the gap between lab- and industrial scale. In this perspective the NPs should also featuring narrow size distribution[8] (standard deviation of the size below 15%), and long-term (optical and colloidal) stability,[9-12] highly desirable for device fabrication.

Since the pioneering work of Protesescu et al.,[13] reporting the synthesis of $CsPbBr_3$ NPs by means of hot-injection (HI) method, many efforts have been put in the fundamental understanding of the dimensional control [14, 15] and enhancement of the optical properties by purposely choosing the reactant composition and/or post-synthesis treatments. Although HI approaches can provide highly luminescent NPs, a fast defocusing of the size distribution within a few seconds from the injection, and shape purity, achievable only in limited temperature range, make the ability to reach narrow size distribution a challenge to be tackled.[8] Furthermore, the use of high-boiling solvent results in detrimental residual solvent traces in the final NP solution, even after the purification. In addition, the energy cost, inherent to the HI method, and the air-free conditions, required for the synthesis, limit the industrial/large scale application of this synthetic approach.

Advantageously, low crystallization energy of this class of materials enables their synthesis by room temperature solution procedures. Ligand-assisted reprecipitation (LARP) stands as the simplest method often put in place in open reactors that, by using basic chemistry apparatus and being inherently scalable, complies the needs for industrial production.[16] However, conventional LARP approach, relying on the use of polar aprotic solvents to dissolve precursors salts and apolar non-solvents for NPs crystallization, suffers from low reaction yield, due to poor solubility of precursor salts (i.e. CsBr and $PbBr_2$).[16] Therefore new approaches have been developed, where salt solubility has been increased by dissolving precursors in apolar aprotic solvents (i.e. toluene) in the presence of solvation agents (i.e. trioctyl phosphine oxide - TOPO - and tetraoctylammonium bromide – TOAB -)[17-21] and ligands.[22] First [17, 18] TOAB has been used as solvation and stabilizing agents, then the addition of less sterically hindered alkyl ammonium bromide has been reported [19] to improve the NP stability. More recently, Brown et

[a] Chemistry Department, University of Bari, via Orabona 4 70126 Bari (IT)
[b] CNR-Institute for chemical physical process (IPCF), via Orabona 4 70126 Bari (IT)
[c] Department of Civil, Environmental, Land, Construction and Chemistry (DICATECh), Polytechnic University of Bari, Via Orabona 4, 70125 Bari (IT)
[d] CNR-Institute of Nanotechnology (Nanotec), Via Monteroni, 73100 Lecce (IT)
[e] National Interuniversity Consortium of Materials Science and Technology, INSTM, Bari Research Unit, 70126, Bari (IT)
Electronic Supplementary Information (ESI) available. See DOI: 10.1039/x0xx00000x

al.[21] employed phosphorous based solvation agents and ligands to afford size control and high emission properties.

NPs surface engineering by a robust passivation layer, indeed, represents a feasible strategy to enhance the emission intensity and limits the material intrinsic lability, that causes optical and structural instability in time.[23]

Although $CsPbBr_3$ is a defect tolerant material, ligand composition has been demonstrated to affect the NP emission properties, making the interplay between NP surface and the ligands shell, and between ligands and the external environment, fundamental keys to obtain robust and highly luminescent NPs for their implementation in technological application. Improvements in electronic passivation,[24, 25] and colloidal stability [26] have been achieved by replacing primary amine ligands [24, 27] with poorly sterically hindered quaternary alkyl ammonium salts,[18, 28] that, instead, cannot, exchange protons.[16, 19, 29-32] Phosphorous based compounds such as alkyl phosphonic acid [21, 33, 34] have been also suggested as robust $CsPbBr_3$ ligands.[20]

Despite numerous efforts, how to concomitantly achieve NP monodispersity, high reaction yield and high emission, and which molecular processes are effectively involved, remain still open issues.

Here we report inherently scalable polar-solvent free LARP approaches aiming at providing highly emissive and monodisperse NPs. To this purpose, *ad-hoc* composition of the reaction mixtures, based on precursors (Cs_2CO_3 and $PbBr_2$), ligands (i.e. oleyl amine, Olam, didodecyl dimethyl ammonium bromide, DDAB or phosphorous compounds in combination with excess of alkyl carboxylic acid, oleic acid, OA, or nonanoic acid, NA), and solvation agents (TOAB or TOPO), jointly with a carefully designed purification process, are investigated. Three distinct series of NPs samples with different ligands labelled NP_{Olam}, NP_{DDAB} and $NP_{OPA\ DDAB}$ are synthesized, and their resulting properties rationalized. The molecular mechanisms underlying the high production yield, the NP size distribution and the time-evolution of the emission properties are clarified for each specific ligands/solvation agent pair, thanks to complementary morphological, spectroscopic, and compositional investigations. Indeed, interesting insights on the molecular control of the NPs properties are gained, thus opening the venue to the implementation of novel cost-effective and scalable synthetic approaches for high quality $CsPbBr_3$ NPs.

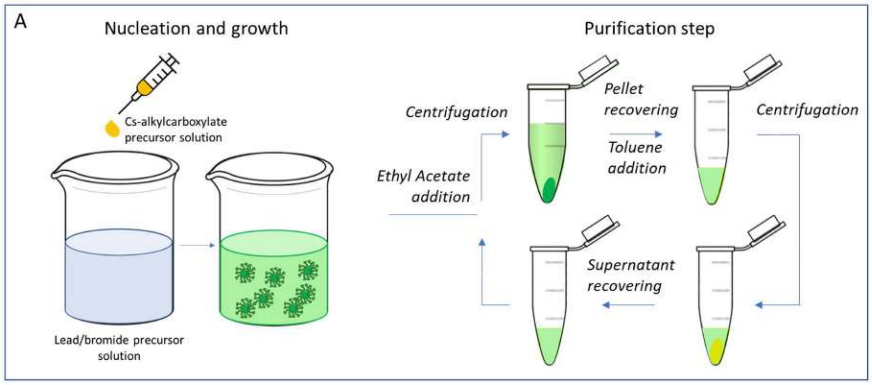

B

Sample	$PbBr_2$: solvation agents/ligands molar ratio	$^*Cs^+$/ligands molar ratio	*Additional Ligands molar ratio	Reaction time seconds	Purification
	$PbBr_2$: TOAB: Olam : OA	$^*Cs^+$: OA	None	120	
NP_{Olam} 1	1 : 1.4: 1.5 : 2.6	0.17:2.5	---		Two-step
NP_{Olam} 2	1 : 1.4: 1.5 : 2.6	0.17:2.5	----		One-step
NP_{Olam} 3	1 : 0.7: 1.5 : 2.6	0.17:2.5			One-step
	$PbBr_2$: TOAB: DDAB : NA	$^*Cs^+$: NA	None	300	
NP_{DDAB} 1	1 : 1.4: 0.60 : 2.6	0.17: 4.6			Two-step
NP_{DDAB} 2	1 : 1.4: 0.15 : 2.6	0.17: 4.6			Two-step
NP_{DDAB} 3	1 : 0.7: 0.30 : 2.6	0.17: 4.6			Two-step
	$PbBr_2$: TOPO: OPA	$^*Cs^+$: NA	DDAB	300	
$NP_{OPA\ DDAB}$ 1	1 : 10: 0.7	0.17: 4.6	0.1		Two-step
$NP_{OPA\ DDAB}$ 2	1 : 10: 0.7	0.17: 4.6	0.1		One step

Figure 1. (A) Schematic illustrations of the synthetic route and purification protocol employed for the room temperature synthesis of $CsPbBr_3$ nanoparticles. (B) Precursor solution composition and synthetic and purification condition used for the synthesis of each NP sample. * The molar ratios values reported are calculated with respect to $PbBr_2$

Results and discussion

Ligand and solvation agents for the synthesis of monodispersed $CsPbBr_3$ NPs. Colloidal $CsPbBr_3$ NPs are synthesized by means of a polar solvent-free LARP approach.[16] According to this procedure, Cs_2CO_3 and $PbBr_2$ precursor salts are separately decomposed at mild reaction temperature, in anhydrous toluene in the presence of solvation and coordinating agents. Unlike for HI methods,[13, 35] here, inert conditions are not required, and precursor decomposition and NP syntheses are carried out in open-air. Then, caesium-precursor is injected at room temperature into the lead/halide

precursor solution, inducing the crystallization of the NPs (Figure 1A), that can be subsequently recovered from the reaction mixture by further addition of an aprotic polar solvent (EtAc) and centrifugation steps. Toluene is finally used as dispersant solvent. The use of toluene as reaction solvent rather than high boiling solvents, generally used in HI, makes purification steps to get rid of left over in the final NP solution less critical.

In order to alleviate the limited solubility of the precursor salt in toluene,[18] solvation agents, like alkylcarboxylic acid (OA or NA) or alkyl phosphine oxide (TOPO), acting as Lewis bases for Cs^+ and Pb^{2+}, respectively, or alkylammonium cation (TOAB) behaving as Lewis acid with halide ions, are added to the precursor solutions. Olam, along with alkylcarboxylic acid, or less sterically hindered alkyl ammonium bromide, such as DDAB, are here tested as ligands.[33, 36-39]

Numerous sets of experiments using distinct ligands' and solvation agents' combination are performed to systematically investigate the role of the reaction mixture composition in the kinetic of NP growth, surface passivation and NP stability, essential for providing a high NP production yield and NPs featuring good monodispersity, long term colloidal and optical stability. A summary of the most relevant preparative conditions is reported in Figure 1B (See Experimental section for NP synthesis and purification details).

All the performed syntheses use a large excess of $PbBr_2$ with respect of caesium ions ($PbBr_2/Cs^+$ = 1/0.17 molar ratio, see Figure 1B) along with halide-rich condition, provided by alkylammonium bromide, i.e. TOAB solvation agents or DDAB ligands, necessary to the formation of highly-coordinated bromoplumbate species, that, by caesium ion intercalation, "template" the perovskite structure. Meanwhile, under these conditions, the occurrence of bromide vacancies at the NP surface is expected to be limited, enhancing optical properties,[40] thanks to improved surface-trap passivation.

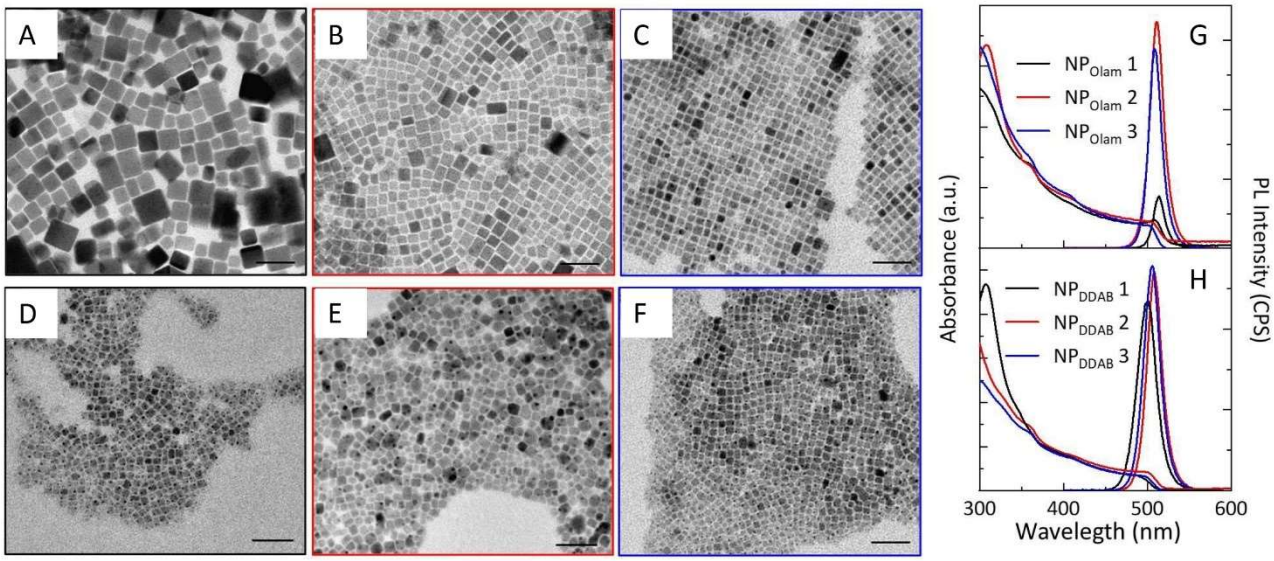

Figure 2. (A-F) TEM micrographs (Scale bar = 50 nm) and (G, H) UV-vis and PL spectra (λ_{ex} = 375 nm) of NP_{Olam} 1-3 (A-C, G) and NP_{DDAB} 1-3 (D-F, H); color code used for micrographs frames corresponds to those reported in panel G and H, respectively

Furthermore, OA or NA, used in excess, react with Olam, when present in the reaction mixtures, shifting the acid-base equilibrium towards the formation of oleyl ammonium bromide, increasing the solubility of the bromide species. OA and NA activate the bromide, due to their reaction with alkylammonium bromide, yielding alkylammonium oleate (nonanoate) and hydrogen bromide. The latter, which is unstable in toluene, leads to additional release of bromide upon decomposition.[41] Figure 2 reports the morphological (Figure 2A-F) and spectroscopic (Figure 2G-H) characterization of the NP_{Olam} (Figure 2A-C, G) and NP_{DDAB} (Figure 2D-F, H) sets of samples whose relevant geometrical features are reported in Figure 3, together with the emission characteristics (emission peak wavelength and relative photoluminescence quantum yield, PL QY). The average lateral size, standard deviation of the size distribution (σ%) (Figure S1 in ESI), absorption extinction coefficient values, as estimated by Equation 1 [42] (see Experimental section), and NP concentration, evaluated by absorption measurement and Lambert-Beer law, allow to estimate the NP production yield.

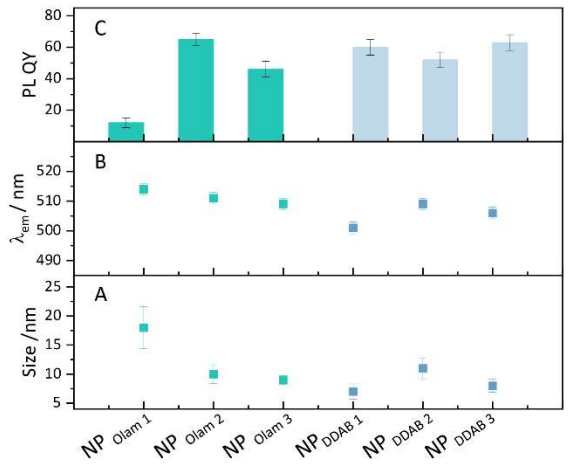

D

Sample name	ε/cm^{-1}*μM^{-1}	NP Concentration /μM
NP_{Olam} 1	141.13	0.0028
NP_{Olam} 2	27.22	0.27
NP_{Olam} 3	16.49	0.60
NP_{DDAB} 1	7.1	0.32
NP_{DDAB} 2	31.4	0.30
NP_{DDAB} 3	13.1	0.45

Figure 3. (A) Scatter plots of nanoparticles' size (error bar size distribution) and (B) emission peak wavelength (λ_{ex}=375 nm) and (C) PLQY value for all the selected samples. (D) Table of molar extinction coefficient ε at λ = 400 nm and concentration of colloidal nanoparticles.

In the case of the NP_{Olam} sample set, regularly shaped nanocubes are obtained (Figure 2A-C). The characterization of these samples, synthesized keeping constant the Olam content, clearly highlights that nanocubes size and monodispersity depend on purification procedure (see NP_{Olam} 1 versus NP_{Olam} 2 and NP $_{Olam}$ 3 Figure 2-3) and TOAB solvation agents' content (see NP_{Olam} 2 versus NP_{Olam} 3 Figure 2-3). It is worth to point out that TOAB loosely coordinates the NP surface, due to steric hindrance of the long four alkyl chains, that place the ammonium positive charge too far from the NP surface to provide adequate stability.[31] Polydisperse (σ=20%) nanocubes (Figure 2A and Figure 3A) with lateral size of 18 nm (NP_{Olam} 1), collected upon two-step purification (see Experimental section), turn into smaller nanocubes (10 nm, σ= 16%, NP_{Olam} 2, and 9nm, σ=9%, NP_{Olam} 3 Figure 2B-C, Figure 3A) when one-step purification is performed. Additionally, a reduction of the nanocubes size distribution, with nearly same average lateral size, is observed for the sample NP_{Olam} 3, synthesized by cutting to half the TOAB content. The large average size and lower NP production yield for NP_{Olam} 1 ([NP_{Olam} 3]> [NP_{Olam} 2]>> [NP_{Olam} 1], Figure 3D) indicate a poor NP stability against purification. Displacement of the ligands at NP surface upon polar solvent addition [43] is expected to take place, which promotes the formation of aggregates, mostly removed by the centrifugation step, resulting in a decrease of the NP production yield. The UV-Vis absorption and emission spectra of NP_{Olam} 1-3 (Figure 2G) show the typical line profile of the $CsPbBr_3$ colloidal solution, and exciton transition and band edge recombination, whose position (Figure 3B) agrees with that expected for weakly quantum-confined NPs of $CsPbBr_3$ (Bohr radius 3.5 nm). The trend in the relative PL QY NP_{Olam} 1<< PL QY NP_{Olam} 3< PL QY NP_{Olam} 2 (Figure 3C) can be discussed by taking into account the role of the size and surface passivation. It is worth to note that spatial confinement of the electron-hole pair, that increases the wave function overlap and the probability of radiative recombination, and trap-assisted recombination of excitons at the surface are competing processes affecting the emission properties and depending on size and surface passivation. Spatial confinement of electron−hole pairs mainly occurs by decreasing NP size, bringing a gradual increase in the NP PL QY as the NPs size decreases.[44, 45] Therefore, NP_{Olam} 1 sample, formed of large nanocubes, presents a low PL QY (12%), ascribable to NP size far from quantum confinement and the possible presence of shallow traps arising from poor passivation (See Figure S2 in ESI). Conversely, higher PL QY value are measured for NP_{Olam} 2 (65 %) and NP_{Olam} 3 (46%) samples, which have, instead, size close to Bohr radius (Figure 3C). It is worth to note that, NP_{Olam} 2 sample, synthesized in the presence of large excess of TOAB, show an absorption band centred at 312 nm, generally ascribed to residual highly coordinating $PbBr_6^{4-}$ species,[46] that is not completely removed after a one-step purification. Such absorption feature is not detected in the spectrum of NP_{Olam} 3 sample, thus suggesting that at lower TOAB content one step purification is sufficient to remove the residual $PbBr_6^{4-}$ intermediates. A bromide-rich condition for NP_{Olam} 2 sample is, hence, expected, which is beneficial for halide vacancies passivation, enhancing radiative recombination path. Indeed, the average PL lifetime of nearly 16.51 ns (±0.2) and 8.80 ns (±0.2), determined by the three-exponential fitting of the PL decay of NP_{Olam} 2 and NP_{Olam} 3, respectively (Figure S2 in ESI), and the corresponding PL QY values suggest a higher density of states involved in radiative recombination for NP_{Olam} 2. Conversely, faster recombination and PL QY< 50% for NP_{Olam} 3 suggest poorly passivated surface trap states.

For the NP_{DDAB} samples, prolonged reaction time (300 s) and lower molar content of DDAB, serving as ligand, are found essential for NP formation and growth. Theoretical investigation and experimental results reported in literature point out that didodecyl dimethyl ammonium ligands are less bulky than TOAB and can effectively bind the NPs surface.[25] This NP ligand coating is more stable than that arising by primary oleylammonium interaction with NPs surface.[47] Moreover, rrecently, it has been pointed out that, since the alkyl ammonium bromides can promptly bind the NPs surface, the higher their concentration, the smaller the NPs.[48] Here, in agreement with these considerations, it is found out that lower reaction time and/or high amount of DDAB do not result in any color change in the solution, indicating that NPs do not form or are too small (data not shown). A large excess of DDAB, promptly binding the NP surface, may hamper the addition of monomers at NP surface, slowing down the kinetic of growth.[28, 49] Conversely to what reported by Song et al.,[19] DDAB needs to be added to the lead/halide precursor solution, to prevent

irreversible aggregation right after caesium injection. NP_{DDAB} 1, synthesized using $PbBr_2$: TOAB: DDAB 1:1.4: 0.6 molar ratio, is characterized by an average lateral size of 7 nm (σ=18%); NP_{DDAB} 2, prepared by reducing only the amount of DDAB ($PbBr_2$: TOAB: DDAB 1:1.4: 0.15), presents larger NPs (11 nm, σ=16%) (Figure 2D-E, Figure 3A). Sample NP_{DDAB} 3, where amount of alkylammonium bromide salts, both TOAB and DDAB ($PbBr_2$: TOAB: DDAB 1:0.7: 0.3 molar ratio, Figure 2F) is reduced, shows NPs with average lateral size of nearly 8 nm (σ=16%). However, irrespectively from the ligands and solvation agents' content, all these samples feature NPs with a broad size distribution (Figure 3). The PL QY, higher than 50%, the reproducible NPs concentration, above 0.3 μM (Figure 3D), estimated for all the samples purified by two-step procedure, prove that the NP_{DDAB} samples are robust against polar solvent (Figure S3 in ESI). DDA^+, featuring two C12 alkyl chains, provides a hydrophobic layer able to effectively protect the NPs surface from the polar solvent and a quaternary ammonium headgroup, that, being not susceptible to protonation, leads to a more stable and robust surface passivation, limiting NPs aggregation and endowing them a high emission.

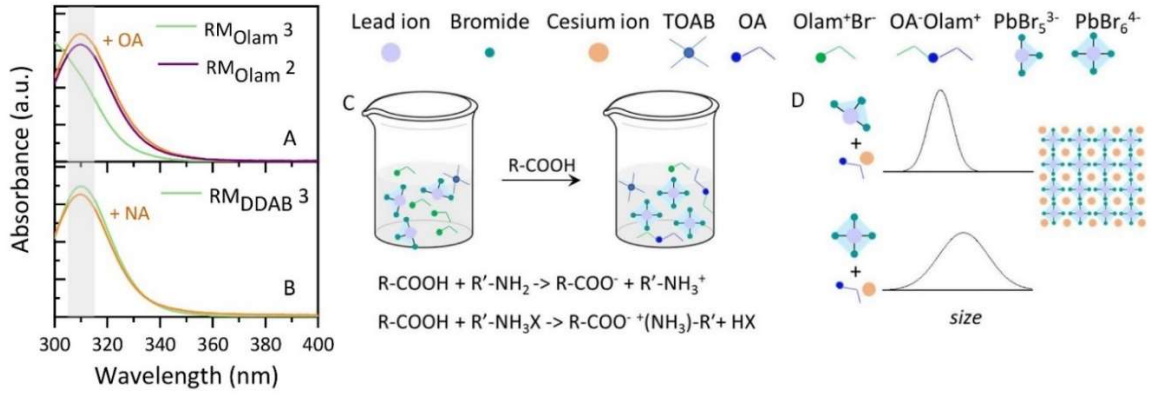

Figure 4. UV absorption spectra of the reaction mixture (RM) used for the preparation of sample NP_{Olam} 2 (violet line, panel A), NP_{Olam} 3 before (green line, panel A) and after (orange line, panel A) addition of oleic acid (OA) solution and NP_{DDAB} 3 before (green line, panel B) and after (orange line, panel B) addition of nonanoic acid (NA) solution. (C) Sketch of the reactions activated by alkyl carboxylic acid (R-COOH) addition in RM_{Olam} 3, triggering the formation of highly coordinated bromoplumbate species. (D) Schematic representation of the condition leading to monodispersed NPs

To this point, it can be concluded that the use of DDAB ligands or large bromide content (NP_{Olam} 2) although able to effectively enhance NPs' PL QY, in fact, leads to a broad size distribution of the NPs. Conversely, the use of Olam, in a proper proportion with TOAB, as solvation agent, brings to the formation of nanocubes with a narrow size distribution, although the labile ligands passivation is responsible of NP aggregation upon addition of polar solvent and decrease of their emission. To further understand how experimental conditions, and in particular, solvation agents and ligands composition, control the NP size distribution, absorption spectra of reaction mixtures (RM) are recorded at the different stages of the synthesis (Figure 4A, B). The spectroscopic characterization can provide the experimental evidences of the bromoplumbate species already in the RM or here released by *in situ* reaction, based on the association of the absorption profile to the specific bromoplumbate species: $PbBr_3^-$ and $PbBr_2$ show an absorption maximum at λ_{max}= ~350 nm, while $PbBr_5^{3-}$ has λ_{max}= 275 nm and $PbBr_6^{4-}$ λ_{max}= 312 nm in organic solvent.[50] The composition in bromoplumbates has been already reported to affect the dimensionality of the NPs,[51, 52] with tridimensional perovskites structures arising from caesium ions intercalation between $PbBr_6^{4-}$ octahedra. To mimick the *in-situ* reaction, avoiding nucleation/crystallization of the NPs, a toluene solution containing the sole OA or NA, at the same concentration used for the caesium precursors, without caesium salt, has been prepared and the proper volume added to the lead/bromide precursor solution either in the presence of Olam or DDAB ligands. Figure 4A shows the absorption spectra of RM of the syntheses of NP_{Olam} 2 (Figure 4A violet line) and NP_{Olam} 3 (Figure 4A green line). While an absorption band at 312 nm, ascribed to $PbBr_6^{4-}$, appears in the RM_{Olam} 2 spectrum, RM_{Olam} 3 reveals an absorption profile that account for the presence of $PbBr_5^{3-}$. However, upon injection of the OA solution (Figure 4A orange line), the spectrum suddenly changes, showing the absorption band characteristic of $PbBr_6^{4-}$. It could be assumed that by the addition of OA solution, more bromide ions are released from the OA reaction with oleyl ammonium bromide, so that the poorly bromide coordinated bromoplumbate species (i.e. $PbBr_5^{3-}$) turns into highly coordinated $PbBr_6^{4-}$, effective for NPs formation (Figure 4C). The replacement of OA with NA, a stronger alkyl carboxylic acid, brings the formation of $PbBr_6^{4-}$ already in the RM_{Olam} 3 (Figure S4) suggesting that the increase in acidity of the alkyl carboxylic acid shifts the equilibria towards the formation of oleylammonium bromides and HBr, bringing to NPs with broad size distribution.

The results of such spectroscopic characterization combined with the outcome of the morphological characterization, indicate a correlation of the concomitant sudden formation of $PbBr_6^{4-}$ and release of caesium ions with the attainment of highly monodispersed NPs as for NP_{Olam} 3 (Figure 4D). Conversely, injection of caesium ions in a solution where $PbBr_6^{4-}$ species are already formed, leads to NPs characterized by broader size distribution as main products (as for NP_{Olam} 2, Figure 4D). This is also confirmed by the NP_{DDAB} series (Figure 4B): even for the RM featuring the lowest TOAB/DDAB content

(RM_{DDAB} 3) the availability of bromide and of lead ions are sufficient to generate $PbBr_6^{4-}$, prior to addition of NA or OA (Figure S4) solution, leading to NPs with a broad size distribution. Here the strength of the alkyl carboxylic acid, does not play any critical role in the regulation of the size distribution, since the bromoplumbates mainly depend on the alkyl ammonium bromide solvation and ligands content.

Time evolution of nanoparticles emission properties.

NP_{Olam} 3 and NP_{DDAB} 3 samples, here named NP_{Olam} and NP_{DDAB} for sake of clarity, are selected since they feature the same size and the higher yield of production among those of the same series. Optical investigation of these samples and of the $NP_{OPA\ DDAB}$ ones, which is synthesized following a polar-solvent free LARP approach reported in literature with minor modification (see Figure S5 in ESI), are performed. The steady-state emission spectra (Figure 5A), PL QY, (Figure 5C), TRPL decays (Figure 5D) of the samples are discussed by considering NP concentration, surface passivation (Figure 6-7), and time evolution of their properties (Figure 8). The high production yield observed for NP_{Olam}, greater than that found for NP_{DDAB} and $NP_{OPA\ DDAB}$ (Figure 5B), can be attributed to the kinetic of NP_{Olam} growth, that is not hampered by strong binding of the ligands.

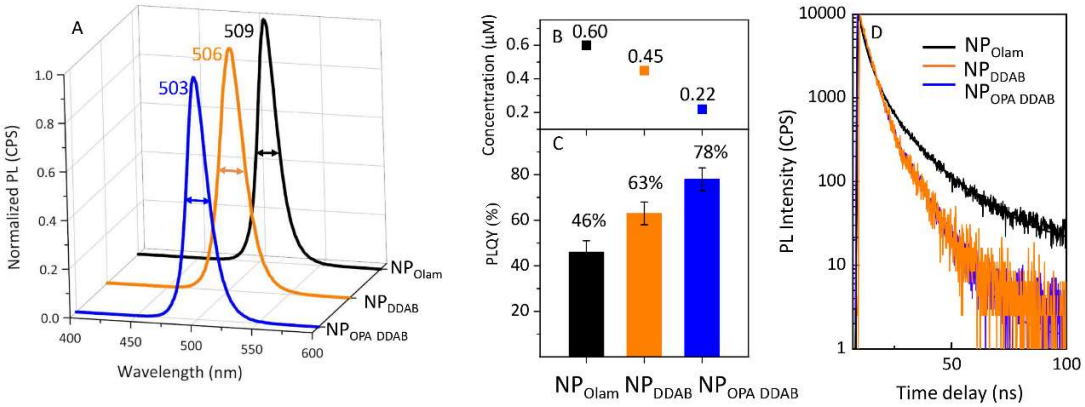

E

Sample	Size nm	σ (%)	Band gap eV	λ_{em} nm	FWHM (meV)	PLQY (%)	<τ> (ns)
NP_{Olam}	9	9	2.38	509	86	46±5	8.8±0.2
NP_{DDAB}	8	14	2.43	506	112	63±3	5.5±0.2
$NP_{OPA\ DDAB}$	8	13	2.42	503	93	78±4	5.3±0.2

Figure 5. UV absorption spectra of the reaction mixture (RM) used for the preparation of sample NP_{Olam} 2 (violet line, panel A), NP_{Olam} 3 before (green line, panel A) and after (orange line, panel A) addition of oleic acid (OA) solution and NP_{DDAB} 3 before (green line, panel B) and after (orange line, panel B) addition of nonanoic acid (NA) solution. (C) Sketch of the reactions activated by alkyl carboxylic acid (R-COOH) addition in RM_{Olam} 3, triggering the formation of highly coordinated bromoplumbate species. (D) Schematic representation of the condition leading to monodispersed NPs

The band gap calculated from the Tauc plot (Figure S6 in ESI) is about 2.43 eV for NP_{DDAB} and $NP_{OPA\ DDAB}$ and slightly smaller (2.38 eV) for the larger NP_{Olam}, thus resulting within the typical range reported for $CsPbBr_3$ NPs and consistent with the size dependence of the band edge or surface passivation (Figure 5E). Emission peak wavelength (Figure 5A) slightly red shifts moving from $NP_{OPA\ DDAB}$, NP_{DDAB} and NP_{Olam} due to size, size distribution and different chemical environment determined by surface capping layer. PL QY values (Figure 5C, $NP_{OPA\ DDAB}$ 78% > NP_{DDAB} 63%> NP_{Olam} 46%) together with PL average lifetimes <τ> (Figure 5D), which exhibit recombination dynamics faster for $NP_{OPA\ DDAB}$ (5.3 ns) and NP_{DDAB} (5.5 ns) than NP_{Olam} (8.8 ns) (Figure 5E), indicate a higher density of radiative states for the $NP_{OPA\ DDAB}$ and NP $_{DDAB}$ samples than NP_{Olam}. Since size effect on the emission properties can be ruled out, due to the quite similar size of the compared samples, such a phenomenon can be thought related to the NPs passivation and stability of the ligands.

To get insight on the NP and ligands shell composition and thus further elucidate NP ligand passivation, Energy Dispersive X-ray Analysis (EDX) analysis are carried out for a semiquantitative determination of the NPs stoichiometry, while a complementary thermogravimetric and NMR characterization investigate the organic molecules composition, either bound or free. Cs: Pb: Br atomic ratio of 0.7: 1: 5 for NP_{Olam}, 1.4: 1: 6 for NP_{DDAB} and 1.5: 1: 7 for $NP_{OPA\ DDAB}$ are calculated from EDX analysis. The resulting Br/Pb ratio > 3 appears consistent with bromide-rich synthetic conditions (Figure S7 in ESI). Although a formal excess of $PbBr_2$ over caesium is always used in the synthesis, NP_{DDAB} and $NP_{OPA\ DDAB}$ show a Cs/Pb ratio slightly higher than 1, while caesium deficient stoichiometry is calculated for NP_{Olam}. Therefore, CsBr-terminated $CsPbBr_3$ NPs[53] can be assumed for NP_{DDAB} and $NP_{OPA\ DDAB}$, being caesium partially replaced by oleyl ammonium ions for NP_{Olam}.[54, 55] Indeed, CsBr termination has been already demonstrated for cuboidal $CsPbBr_3$ nanocrystals, as the more thermodynamically

favoured surface for NPs in the size range between 7-11 nm.[53] In fact, within this size regime, $PbBr_2$ termination is unlikely to occur as it would requires much denser ligand packing, that would encounter significant steric hindrance, with the consequent disruption of the Pb^{2+} octahedral coordination.[53]
Thermogravimetric (TG) analysis has been performed under nitrogen flow on each NP sample collected as pellet after purification and drying at 50°C, by applying a heating ramp from 50 °C to 700°C. TG and first derivative (DTG) curves are reported in Figure 6. Above 550°C, the weight loss could be reasonably ascribed to the $CsPbBr_3$ decomposition,[56, 57] while the thermal events in the 50°C and 550 °C temperature range arise from degradation of the tightly or weakly bound organic molecules of the NP shell. TG analysis can provide qualitative and quantitative information on the composition of the NP ligands and surface coverage by comparing the TG profile with those of pure ligands and solvation agents [58, 59] used as reference (Figure S8 in ESI and table in Figure 6A). The evaporation of ligands chemically bound to the NP surface results in weight losses at high temperature and with a typically broaden TG profile.[58, 60] A total weight loss of 35 wt% has been calculated for $NP_{OPA\ DDAB}$, while NP_{Olam} and NP_{DDAB} show nearly 15wt% and 12wt%, respectively. Since both $NP_{OPA\ DDAB}$ and NP_{Olam} underwent to the same one-step purification, the high weight loss for $NP_{OPA\ DDAB}$ can be attributed to residual molecules more resistant to removal by purification solvent. NP_{Olam} weight loss occurred in two temperature ranges: a first one between 175-263°C, marked by a peak in the DTG curve centred at 236 °C (Figure 6B), and a second one between 265-400 °C, with major evaporation peak at 356°C (Figure 5B). Even though the TG profile does not allow to discriminate between OA and Olam, the first weight loss could be associated with the elimination of free or physically adsorbed ligands, while the second one, covering a higher temperature range, to weight loss ascribed to evaporation of ligands bound to the surface of the NPs.[58]

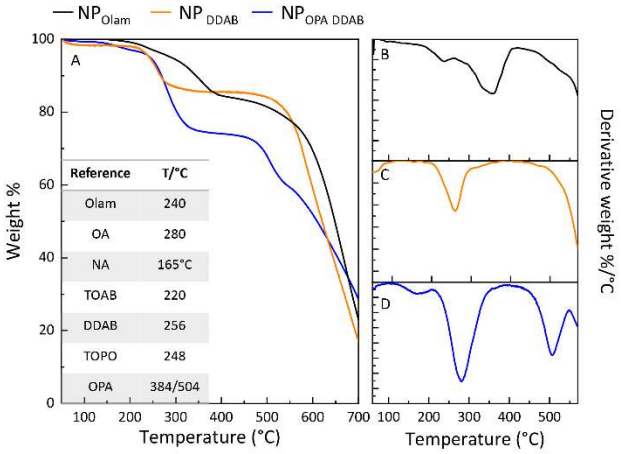

Figure 6. (A) Thermogravimetric and (B-D) first derivative curves of NPOlam, NP_{DDAB}, $NP_{OPA\ DDAB}$ and table with evaporation temperature onset for pure ligands as reference in panel A.[58, 59]

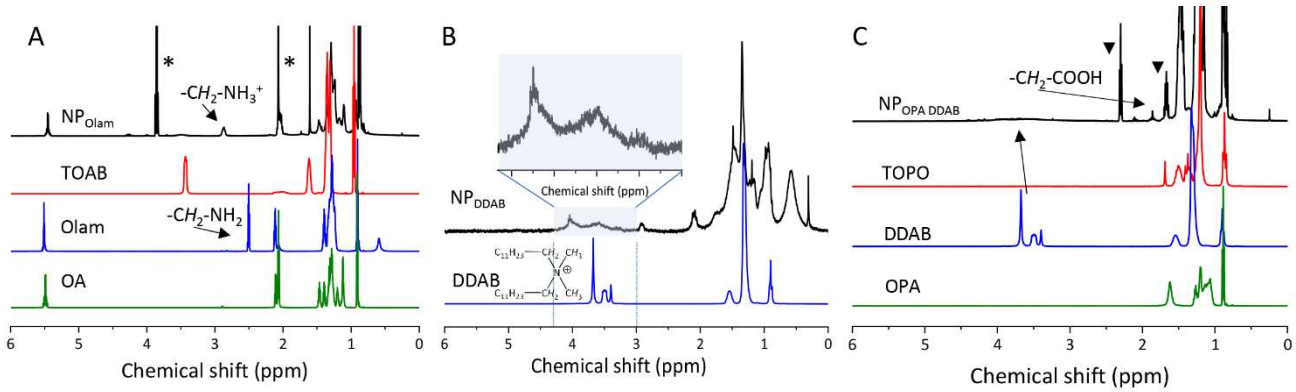

Figure 7 1H-NMR spectra of the nanoparticles (black line) along with those of the solvation agents and ligands used during the synthesis as reference. * indicates the peaks belonging to residual ethyl acetate (used for the purification stage). ▼ indicates the signals tentatively attributable to polyphosphonic anhydrides

The presence of residual free TOAB could not be ruled out in the NP_{Olam} sample nor in the NP_{DDAB} sample. This latter sample shows a single weight loss (nearly 12%) in the range from 225 °C and 280°C, marked by a peak at 260°C, associated to the loss of the DDAB bound to the NP surface. Weight losses over the ranges of 150-200°C (4%) , 228-330 °C (20%) and the steep one between 475 -530°C (11%) are shown for $NP_{OPA\ DDAB}$, ascribed to the evaporation of NA, DDAB and TOPO, OPA,[61] respectively (Figure S8 in ESI).
The comparison of the ^{1}H-NMR spectra of the NPs in C_6D_6 with those of the ligands and solvation agents provides relevant insights in NP surface passivation. Signal broadening is due to ligands interacting with the NPs' surface, which causes a slower mobility in solution compared to corresponding free ligands.[62, 63] The ^{1}H NMR spectrum of NP_{Olam} sample clearly shows the broad resonances of the methylene protons α-CH_2- of Olam in the 2.8-2.9 ppm range, with resonance being broadened and shifted downfield compared to free oleyl amine as expected from bound oleylammonium (Figure 6A). The ^{1}H NMR spectrum indicates that Olam is partially protonated, while OA, whose characteristic resonances preserve the fine structure at exactly the same chemical shift as free molecule, is not bound to the NP

surface and it is still protonated. The ^{1}H NMR spectra of NP_{DDAB} (Figure 6B) and $NP_{OPA\ DDAB}$ (Figure 6C) show a broad signal in the 3.2 to 4.1 ppm range, belonging to surface-bound DDA^{+} molecule. The chemical shifts of these broad peaks at lower field compared to those of free DDAB molecules [32] are due to the different solvation at the surface of the NPs. Furthermore, the NMR spectrum of $NP_{OPA\ DDAB}$ sample features multiple peaks in the range of 1.8-2.4 ppm tentatively attributed to polyphosphonic anhydrides that may have formed by condensation of phosphonic acids during the synthesis. It can be noted that the NMR spectrum of $NP_{OPA\ DDAB}$ does not show any signals ascribed to TOPO. This result suggests that it is largely removed by purification, though traces of TOPO cannot be ruled out. Residual NA, not adsorbed to the NP surface, is also detected, confirming the TGA characterization.

Following the nomenclature proposed by Bodnarchuk et al.,[24] the NPs can be conveniently written as $[CsPbBr_3](PbBr_2)_n\{AX\}_n$ structure where $[CsPbBr_3]$ is the inner core terminated by a $(PbBr_2)$ inner shell and a {AX} outer shell. The outer {AX} shell is composed of two types of A cations, Cs^{+} and didodecyl dimethylammonium (DDA^{+}), with a slight excess of caesium ions for $NP_{OPA\ DDAB}$ and NP_{DDAB} and Cs^{+} and oleyl ammonium, with a slight excess of oleylammonium for NP_{Olam}, and X type anions mainly Br^{-}. The lower PL QY for NP_{Olam} can be attributed to labile binding of oleylammonium.[36] On the other hand, DDAB,[24, 64] passivating the surface of $NP_{OPA\ DDAB}$ and NP_{DDAB}, as Z-type ligands,[65] which could not lose or acquired protons, is capable of leading to a marked improvement of the NP stability, resulting in highly emissive NPs.

The time evolution of the PL QY and the PL recombination dynamics (Figure 8 and Figure S9-S11) are monitored in time to evaluate the possible role of the specific surface chemistry on the modification of the emission properties. In principle, the ligands' dynamic exchanges and reactions with the environment can be assumed responsible of such evolution. The emission properties, being strongly correlated to the surface passivation, may provide the prompt optical evidence of mechanisms at the molecular/interface level that may affect the stability of NPs, or, alternatively, display how to limit them. Emission peak wavelength (Figure 8A) remains unchanged for NP_{Olam} and $NP_{OPA\ DDAB}$, while a blue shift is measured for NP_{DDAB}, suggesting modification of the average size and/or size distribution. Statistical analysis of TEM micrographs (Figure S12) of this sample after 90 days of storage in air, indeed, reveals that NPs preserved the average lateral size (8 nm), assuming a more regular cuboidal structure than pristine ones, with narrower size distribution (from σ%=14% to σ%=10%).

In general, the emission properties of NP_{Olam} remain surprisingly unchanged after being stored in air for 90 days, unlike the generally reported deterioration of optical properties due to displacement of oleyl ammonium bromide caused by deprotonation. An explanation of this behaviour can be seen in the presence of residual free oleic acid molecules that sustain a large availability of oleylammonium bromide and limit its possible detachment from the NP surface upon air/humidity exposure (Scheme 1A). A marked increase in the PL QY (from 63% up to 88%, Figure 8B) and of the PL lifetime (Figure 8C) is observed for NP_{DDAB}, characterized by bound DDAB and free TOAB/DDAB molecule, which suggests a better surface passivation. Imran et al. [31] reported a PL QY increase and a concomitant shrinking of the NP size upon addition of DDAB, explaining these findings to the exchange reaction of DDAB with NP outer shell components. A similar explanation can be here proposed for the investigated NP_{DDAB}. Over the time, residual free DDAB can replace surface Cs-X, leading to a higher density of DDAB molecules binding the NP surface (Scheme 1B). This turns in an enhanced passivation with organic shell resistant to ambient condition, and an increase of the PL QY, while leading to a narrowing of the size distribution (Figure S 12). On the other hand, the PLQY of the $NP_{OPA\ DDAB}$, though remaining high, decreases from 78% to 68% after 3 months (Figure 8B). The in-depth investigation of carrier dynamics (Figure 8C) reveals a decrease of the PL QY, an almost preserved average PL lifetime that suggest dominance of non-radiative processes over radiative ones in time, due to modification of the surface passivation and formation of surface trap-states. Simulations and empirical evidence reported by Zaccaria et al.[32] demonstrated that treatments with exogenous alkyl phosphonic and carboxylic acid molecule induce the stripping of DDA^{+} form DDAB-passivated NPs, with a quenching of the luminescence. Similarly, it can be assumed that free protic NA (Scheme 1C), shown in the $NP_{OPA\ DDAB}$ by the TGA and NMR characterization, can displace DDA^{+} reducing ligand density and thus leading to trap states formation. Indeed, adsorption of NA as neutral L-ligands to Cs or Pb sites is not expected to occur, being an endergonic process. On the other hand, NA interaction as L^{-} replacing bromide as HBr cannot be expected either, as not favoured due to the higher pKa (4.9) of NA than HBr.[32]

.

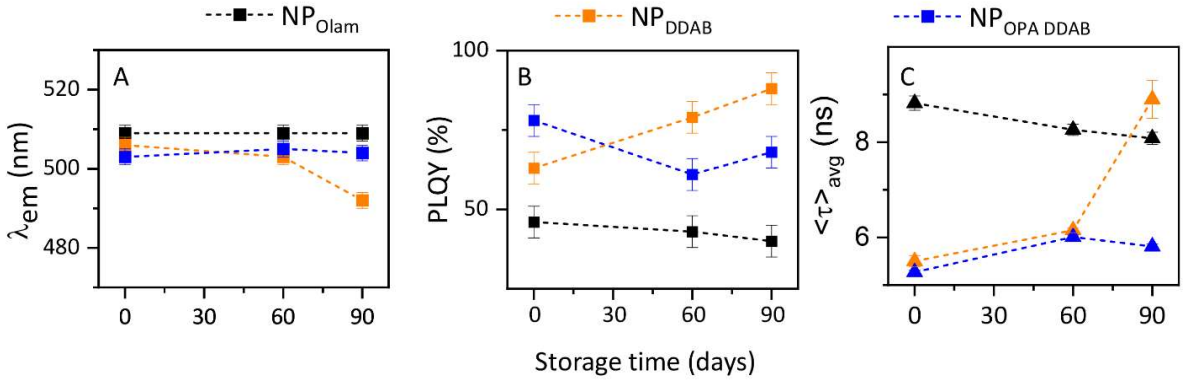

.

Figure 8. Time evolution of (A) emission peak wavelength, (B) PL QY, (C) average PL lifetime ($<\tau>_{avg}$) for NP_{Olam} (black line), NP_{DDAB} (orange line) and $NP_{OPA\ DDAB}$ (blue line).

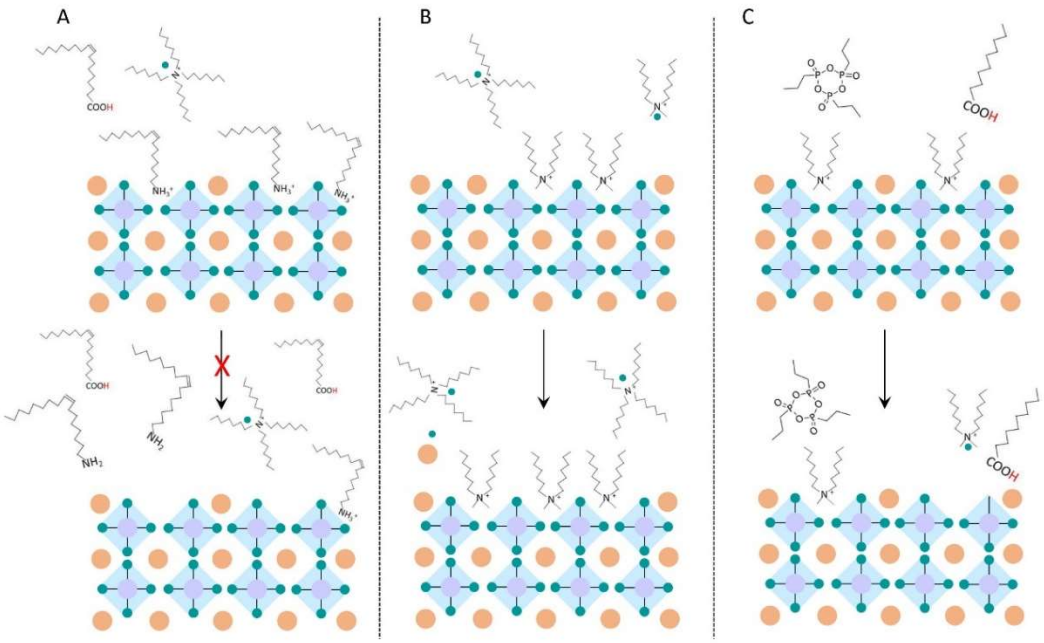

Scheme 1. Schematic representation of the dynamic time evolution of NPs ligands composition and stabilization

Conclusions

Here, room temperature LARP approaches in non-polar solvent in air have been developed, defining for each pair of ligands/solvation agents the reaction mixtures most suited to obtain high NPs production yield and NPs featuring enhanced emission.

The concomitant release of highly coordinated bromoplumbates species and caesium ions has been proved to lead monodispersed samples; fast growth, not hampered by ligands strongly bound or ligands tolerant to purification treatments, have been demonstrated to favour high production yield. Residual species in the NPs colloidal solution have been found to affect, over long-time scale, the ligand shell stability, by taking part in reactions that can increase NPs surface passivation or promote ligands displacements, affecting time-evolution of the emission properties.

The overall study has provided a deep insight into the complex molecular processes involved in the control of size, reaction yield and emission properties of colloidal $CsPbBr_3$ NPs, in view of the development of up-scale procedures offering high quality materials for effective implementation in relevant technological applications.

Experimental section

Materials. $PbBr_2$ (98%), Cs_2CO_3 (Alfa Aesar, 99.9%), nonanoic acid (NA, Sigma Aldrich, technical grade, 96%), oleic acid (OA, Sigma Aldrich, technical grade, 90%), oleyl amine (Olam, Sigma Aldrich, technical grade, 70%), didodecyl dimethylammonium bromide (DDAB, Sigma Aldrich, technical grade, 98%), octylphosphonic acid (OPA, 98%), trioctylphosphine oxide (TOPO, Sigma Aldrich, technical grade, 90%), anhydrous toluene (Sigma Aldrich, 99.8%), ethyl acetate (EtAc, Sigma Aldrich, 99.8%).

Caesium precursor solution. Cs_2CO_3 (32.6 mg, 0.1 mmol) was dissolved in 1 ml of OA (3 mmol) or NA (5.6 mmol). The solution was heated at 80°C in open air and stirred for 1 hour prior to its use. The Cs-oleate (0.2 M) and Cs-nonanoate (0.2 M) precursor solution was used for the synthesis of $CsPbBr_3$ NPs.

Synthesis and purification of $CsPbBr_3$ NP_{Olam}. A lead/bromide precursor solution was prepared by adding 165.2 mg (0.45 mmol) of $PbBr_2$, 330 mg (0.6 mmol) of TOAB and 360 µL (1.15 mmol) of OA to 3 ml of toluene resulting in $[PbBr_2]$ = 0.13 M, [TOAB] = 0.18 M, [OA]=0.34 M. A second precursor solution was prepared by adding the same amount of $PbBr_2$ and OA, cutting to half the TOAB final concentration, 0.09 M. The precursor solution was heated at 70°C for 15 min. For the synthesis of $CsPbBr_3$ NPs, 34 µL of a solution of Olam in toluene (0.3 M, 0.01 mmol) were added to 0.5 mL of each $PbBr_2$ precursor solution, followed by the injection of 55 µL of the Cs-oleate solution (11 µmol) under vigorous stirring at room temperature. Syntheses were also carried out from lead/bromide precursor solution prepared with NA, instead of OA, injecting Cs-nonanoate (Figure S2). After a further 120 s, EtAc was added as non-solvent to precipitate the NPs.

Two purification procedures were tested to remove unreacted by-products and excesses of ligands and collect the NPs, namely a two-step and a single-step procedure.

For the two-step procedure, in the first stage, EtAc was added to the reaction mixture at a 3:1 v/v ratio and then the colloidal dispersion was centrifuged at 10000 rpm for 10 minutes; the

supernatant was discarded, and the precipitate was redispersed in 100 µL of toluene, followed by a second step of centrifugation at 5000 rpm. At this stage the supernatant was recovered for the second purification step. Finally, the pellet was redispersed in 1 mL of toluene.

For the one-step purification, a reaction mixture: EtAc 1:6 v/v ratio was used, and the NPs were collected by following the cycles of centrifugation/redispersion in toluene as previously described. These samples were labelled NP_{Olam}.

Synthesis and purification of $CsPbBr_3$ NP_{DDAB}. The lead/bromide precursor solution was prepared by adding 165.2 mg (0.45 mmol) of $PbBr_2$, 200 µL NA (1.15 mmol) and 330 mg (0.6 mmol) of TOAB to 3 ml of toluene, resulting in [$PbBr_2$] = 0.14 M, [TOAB] = 0.19 M, [NA]=0.36 M (or OA, at the same concentration). A second precursor solution was prepared by cutting to half the TOAB (0.09 M). The precursor solution was heated at 70°C for 15 min. For the synthesis of the NPs, 15 mg (32.4 µmol) or 5 mg (10.8 µmol) or 10 mg (21.6 µmol) of DDAB were added to 0.5 ml of the lead/bromide precursor solution. The mixture was stirred at room temperature until DDAB completely dissolved. Then, 55 µL of the Cs-nonanoate solution (11 µmol) was quickly injected under vigorous stirring and the solution was let stirring for 300 s. Shorter reaction time of 120 s was also tested. The two-step purification procedure was used to recover the NPs, remove the unreacted precursors and ligands, finally dispersing the NPs in 1 mL of toluene. These samples were labelled NP_{DDAB}.

Synthesis and purification of $CsPbBr_3$ $NP_{OPA\ DDAB}$. The synthesis was carried out according to the procedure reported by Brown et al.[21] with minor modifications. $PbBr_2$ 165.2 mg (0.45 mmol) was dissolved in toluene (3 mL) in the presence of TOPO (1.7 g, 4.5 mmol) and the flask was heated at 70°C for 15 min prior to the addition of OPA (58 mg, 0.3 mmol). The precursor solution results in [$PbBr_2$] = 0.15 M, [TOPO] = 0.15 M, [OPA]=0.1 M. Cs-nonanoate solution (55 µL, 11 µmol) was injected in 0.5 mL of the lead/bromide precursor solution. After 30 s, 156 µL of a DDAB solution in toluene (0.05 M, 0.008 mmol) was added and after a further 300 s, the NP were recovered by addition of EtAc. A two-step and one-step purification procedures were performed. In particular, the one-step procedure was investigated by tuning the EtAc to reaction mixture v/v ratio at a 3:1, 1.5: 1, 1:1. The collected NPs were diluted to 1 mL of toluene. These samples were labelled $NP_{OPA\ DDAB}$.

Transmission electron microscopy (TEM). TEM micrographs were acquired with a JEOL JEM1011 electronic microscope operating at 100 kV, equipped with a high-resolution CCD camera. Carbon-coated copper grids were dipped in the NPs colloidal solution diluted 1:20 with toluene letting the solvent to evaporate.

UV-Vis spectroscopy. UV-Vis-NIR absorption spectra of all $CsPbBr_3$ NP samples were measured in 1 cm path length quartz cuvettes using a Cary Varian 5000 spectrophotometer supplied with a double detector. The absorption coefficient ϵ was calculated as reported by Maes, J., et al.,[42] according to the following equation:

$$\varepsilon = \frac{N_A \mu_i}{ln10} d^3 \qquad \text{(Eq.1)}$$

where μ_i is the intrinsic absorption coefficient and d the average diameter, as calculated from TEM analysis.

Steady State PL and Time-Resolved Photoluminescence Measurements. Steady-state photoluminescence (PL) spectra and time resolved photoluminescence (TRPL) measurements were recorded for $CsPbBr_3$ colloidal solution having an optical absorption below 0.15. A HORIBA Jobin-Yvon Fluorolog 3 spectrofluorometer, equipped with double grating excitation and emission monochromators, was used to record PL spectra, using an excitation wavelength at 375 nm, and TRPL measurements. The latter were carried out by using the Time-Correlated Single Photon Counting (TCSPC) technique using a picosecond laser diode (NanoLED 375L, excitation at 375 nm), with a pulse length of 80 ps and 1 MHz repetition rate. The PL signals were dispersed by a double grating monochromator and detected by a picosecond photon counter (TBX Photon Detection Module, HORIBA Jobin-Yvon). The time resolution of the experimental set up was ~200 ps.

The relative PL quantum yield of the $CsPbBr_3$ samples was estimated using Coumarin 153 in ethanol as standard reference, including the correction for solvent refractive indices at 375 nm excitation wavelength, within the ratio calculation. The PLQY of Coumarin 153 in ethanol is taken as 38%.[66]

Nuclear Magnetic Resonance (NMR). ^{1}H-NMR spectra were recorded on Agilent 500/54 Premium shielded spectrometer. ^{1}H chemical shifts were referenced using the internal residual peak of the solvent (C_6D_6, δ 7.16 ppm).

Thermogravimetric analysis (TGA). TGA was carried out using a Pyris 1-Perkin Elmer instrument under a nitrogen flow of 40 mL/min at the heating rate of 20 °C/min in a temperature range from 50°C to 700°C. Thermograms were collected using powder of dried NP samples.

EDX Analysis. Elemental analyses of the powders were performed by Energy Dispersive X-ray Analysis (EDX) on a Field Emission Sigma Zeiss SEM microscope (ZEISS, ΣIGMA) equipped with a LaB_6 source thermal field emitter and a Gemini objective lens. The samples for EDX characterization were prepared by drop casting the NPs colloidal dispersion solutions onto an extensively washed silica substrate. The measurements were performed at working distance of 7 mm and an electron generation voltage of 15 keV.

Author contribution

Ms. M. Giancaspro: conceptualisation, investigation, visualisation, writing – original draft; Prof. R. Grisorio: investigation, writing – original draft and writing – review and editing; Mr. G. Alò: investigation, visualization; Prof. N. Margiotta: investigation, visualisation, writing – review and editing; Dr. A. Panniello: supervision, visualization, writing – review and editing; Prof. G. P. Suranna: visualization, writing – review and editing; Dr. N. Depalo: visualization, writing – review and editing Dr. M. Striccoli: visualization, funding acquisition and writing – review and editing; Prof. M. L. Curri: visualization, funding acquisition and writing – review and editing; Prof. E. Fanizza: conceptualisation, supervision, investigation, visualisation, writing – original draft, and writing – review and editing.

Conflicts of interest

There are no conflicts to declare.

Acknowledgements

The authors thank Dr. R. Castaldo and Dr. G. Gentile, from CNR-Institute of Polymers, Composites and Biomaterials (CNR-IPCB) for support and fruitful discussion in thermogravimetric analysis. The Italia PON R&I ECOTEC (2014–2020 ARS01_00951) and the Project titiled "Network 4 Energy Sustainable Transition – NEST", project code PE0000021, Concession Decree No. 1561 of 11.10.2022 adopted by Ministero dell'Università e della Ricerca (MUR), CUP B53C22004060006, funded by the European Union– NextGenerationEU under the National Recovery and Resilience Plan (NRRP), Mission 4 Component 2 Investment 1.3 - Call for tender No. 1561 of 11.10.2022 of Ministero dell'Università e della Ricerca (MUR) are grateful acknowledged.

References

1. M. V. Kovalenko, L. Protesescu and M. I. Bodnarchuk, Properties and potential optoelectronic applications of lead halide perovskite nanocrystals, *Science (New York, N.Y.)*, 2017, **358**, 745-750.
2. H. Huang, M. I. Bodnarchuk, S. V. Kershaw, M. V. Kovalenko and A. L. Rogach, Lead Halide Perovskite Nanocrystals in the Research Spotlight: Stability and Defect Tolerance, *ACS Energy Letters*, 2017, **2**, 2071-2083.
3. Q. A. Akkerman, G. Rainò, M. V. Kovalenko and L. Manna, Genesis, challenges and opportunities for colloidal lead halide perovskite nanocrystals, *Nature Materials*, 2018, **17**, 394-405.
4. J. Cui, Y. Liu, Y. Deng, C. Lin, Z. Fang, C. Xiang, P. Bai, K. Du, X. Zuo, K. Wen, S. Gong, H. He, Z. Ye, Y. Gao, H. Tian, B. Zhao, J. Wang and Y. Jin, Efficient light-emitting diodes based on oriented perovskite nanoplatelets, *Science advances*, 2021, **7**, eabg8458.
5. M. Liu, Q. Wan, H. Wang, F. Carulli, X. Sun, W. Zheng, L. Kong, Q. Zhang, C. Zhang, Q. Zhang, S. Brovelli and L. Li, Suppression of temperature quenching in perovskite nanocrystals for efficient and thermally stable light-emitting diodes, *Nature Photonics*, 2021, **15**, 379-385.
6. J. Wang, Y. Xu, S. Zou, C. Pang, R. Cao, Z. Pan, C. Guo, S. Hu, J. Liu, Z. Xie and Z. Gong, Effective defect passivation of CsPbBr3 quantum dots using gallium cations toward the fabrication of bright perovskite LEDs, *Journal of Materials Chemistry C*, 2021, **9**, 11324-11330.
7. L. Cheng, J. Chi, M. Su and Y. Song, Interface engineering of perovskite nanocrystals: challenges and opportunities for biological imaging and detection, *Journal of Materials Chemistry C*, 2023, DOI: 10.1039/D2TC04967H.
8. G. Almeida, L. Goldoni, Q. Akkerman, Z. Dang, A. H. Khan, S. Marras, I. Moreels and L. Manna, Role of Acid–Base Equilibria in the Size, Shape, and Phase Control of Cesium Lead Bromide Nanocrystals, *ACS Nano*, 2018, **12**, 1704-1711.
9. R. Grisorio, F. Fasulo, A. B. Muñoz-García, M. Pavone, D. Conelli, E. Fanizza, M. Striccoli, I. Allegretta, R. Terzano, N. Margiotta, P. Vivo and G. P. Suranna, In Situ Formation of Zwitterionic Ligands: Changing the Passivation Paradigms of CsPbBr3 Nanocrystals, *Nano Letters*, 2022, **22**, 4437-4444.
10. E. Fanizza, F. Cascella, D. Altamura, C. Giannini, A. Panniello, L. Triggiani, F. Panzarea, N. Depalo, R. Grisorio, G. P. Suranna, A. Agostiano, M. L. Curri and M. Striccoli, Post-synthesis phase and shape evolution of CsPbBr3 colloidal nanocrystals: The role of ligands, *Nano Research*, 2019, **12**, 1155-1166.
11. Y. Zhang, G. Li, C. She, S. Liu, F. Yue, C. Jing, Y. Cheng and J. Chu, Room temperature preparation of highly stable cesium lead halide perovskite nanocrystals by ligand modification for white light-emitting diodes, *Nano Research*, 2021, **14**, 2770-2775.
12. M. Pols, T. Hilpert, I. A. W. Filot, A. C. T. van Duin, S. Calero and S. Tao, What Happens at Surfaces and Grain Boundaries of Halide Perovskites: Insights from Reactive Molecular Dynamics Simulations of CsPbI3, *ACS Applied Materials & Interfaces*, 2022, **14**, 40841-40850.
13. L. Protesescu, S. Yakunin, M. I. Bodnarchuk, F. Krieg, R. Caputo, C. H. Hendon, R. X. Yang, A. Walsh and M. V. Kovalenko, Nanocrystals of Cesium Lead Halide Perovskites (CsPbX3, X = Cl, Br, and I): Novel Optoelectronic Materials Showing Bright Emission with Wide Color Gamut, *Nano Letters*, 2015, **15**, 3692-3696.
14. X. Zheng, Y. Hou, H.-T. Sun, O. F. Mohammed, E. H. Sargent and O. M. Bakr, Reducing Defects in Halide Perovskite Nanocrystals for Light-Emitting Applications, *The Journal of Physical Chemistry Letters*, 2019, **10**, 2629-2640.
15. C. Otero-Martínez, D. García-Lojo, I. Pastoriza-Santos, J. Pérez-Juste and L. Polavarapu, Dimensionality Control of Inorganic and Hybrid Perovskite Nanocrystals by Reaction Temperature: From No-Confinement to 3D and 1D Quantum Confinement, *Angewandte Chemie International Edition*, 2021, **60**, 26677-26684.
16. A. A. M. Brown, B. Damodaran, L. Jiang, J. N. Tey, S. H. Pu, N. Mathews and S. G. Mhaisalkar, Lead Halide Perovskite Nanocrystals: Room Temperature Syntheses toward Commercial Viability, *Advanced Energy Materials*, 2020, **10**, 2001349.
17. S. Wei, Y. Yang, X. Kang, L. Wang, L. Huang and D. Pan, Room-temperature and gram-scale synthesis of CsPbX3 (X = Cl, Br, I) perovskite nanocrystals with 50–85% photoluminescence quantum yields, *Chemical Communications*, 2016, **52**, 7265-7268.
18. S. Wei, Y. Yang, X. Kang, L. Wang, L. Huang and D. Pan, Homogeneous Synthesis and Electroluminescence Device of Highly Luminescent CsPbBr3 Perovskite Nanocrystals, *Inorganic Chemistry*, 2017, **56**, 2596-2601.
19. J. Song, J. Li, L. Xu, J. Li, F. Zhang, B. Han, Q. Shan and H. Zeng, Room-Temperature Triple-Ligand Surface Engineering Synergistically Boosts Ink Stability, Recombination Dynamics, and Charge Injection toward EQE-11.6% Perovskite QLEDs, *Advanced Materials*, 2018, **30**, 1800764.
20. K. Dave, Z. Bao, S. Nakahara, K. Ohara, S. Masada, H. Tahara, Y. Kanemitsu and R.-S. Liu, Improvement in quantum yield by suppression of trions in room temperature synthesized CsPbBr3 perovskite quantum dots for backlight displays, *Nanoscale*, 2020, **12**, 3820-3826.
21. A. A. M. Brown, P. Vashishtha, T. J. N. Hooper, Y. F. Ng, G. V. Nutan, Y. Fang, D. Giovanni, J. N. Tey, L. Jiang, B. Damodaran, T. C. Sum, S. H. Pu, S. G. Mhaisalkar and N. Mathews, Precise Control of CsPbBr3 Perovskite

Nanocrystal Growth at Room Temperature: Size Tunability and Synthetic Insights, *Chemistry of Materials*, 2021, **33**, 2387-2397.

22. C. M. Guvenc, A. Kocabas and S. Balci, Polar solvent-free room temperature synthesis of CsPbX3 (X = Br, Cl) perovskite nanocubes, *Journal of Materials Chemistry C*, 2023, **11**, 3039-3049.
23. W. Yan, J. Shen, Y. Zhu, Y. Gong, J. Zhu, Z. Wen and C. Li, CsPbBr3 quantum dots photodetectors boosting carrier transport via molecular engineering strategy, *Nano Research*, 2021, **14**, 4038-4045.
24. M. I. Bodnarchuk, S. C. Boehme, S. ten Brinck, C. Bernasconi, Y. Shynkarenko, F. Krieg, R. Widmer, B. Aeschlimann, D. Günther, M. V. Kovalenko and I. Infante, Rationalizing and Controlling the Surface Structure and Electronic Passivation of Cesium Lead Halide Nanocrystals, *ACS Energy Letters*, 2019, **4**, 63-74.
25. J. H. Park, A.-y. Lee, J. C. Yu, Y. S. Nam, Y. Choi, J. Park and M. H. Song, Surface Ligand Engineering for Efficient Perovskite Nanocrystal-Based Light-Emitting Diodes, *ACS Applied Materials & Interfaces*, 2019, **11**, 8428-8435.
26. D. Quarta, M. Imran, A.-L. Capodilupo, U. Petralanda, B. van Beek, F. De Angelis, L. Manna, I. Infante, L. De Trizio and C. Giansante, Stable Ligand Coordination at the Surface of Colloidal CsPbBr3 Nanocrystals, *The Journal of Physical Chemistry Letters*, 2019, **10**, 3715-3726.
27. S. ten Brinck, F. Zaccaria and I. Infante, Defects in Lead Halide Perovskite Nanocrystals: Analogies and (Many) Differences with the Bulk, *ACS Energy Letters*, 2019, **4**, 2739-2747.
28. W. Zheng, Z. Li, C. Zhang, B. Wang, Q. Zhang, Q. Wan, L. Kong and L. Li, Stabilizing perovskite nanocrystals by controlling protective surface ligands density, *Nano Research*, 2019, **12**, 1461-1465.
29. M. Imran, P. Ijaz, D. Baranov, L. Goldoni, U. Petralanda, Q. Akkerman, A. L. Abdelhady, M. Prato, P. Bianchini, I. Infante and L. Manna, Shape-Pure, Nearly Monodispersed CsPbBr3 Nanocubes Prepared Using Secondary Aliphatic Amines, *Nano Letters*, 2018, **18**, 7822-7831.
30. Y. Miao, Y. Chen, H. Chen, X. Wang and Y. Zhao, Using steric hindrance to manipulate and stabilize metal halide perovskites for optoelectronics, *Chemical Science*, 2021, **12**, 7231-7247.
31. M. Imran, P. Ijaz, L. Goldoni, D. Maggioni, U. Petralanda, M. Prato, G. Almeida, I. Infante and L. Manna, Simultaneous Cationic and Anionic Ligand Exchange For Colloidally Stable CsPbBr3 Nanocrystals, *ACS Energy Letters*, 2019, **4**, 819-824.
32. F. Zaccaria, B. Zhang, L. Goldoni, M. Imran, J. Zito, B. van Beek, S. Lauciello, L. De Trizio, L. Manna and I. Infante, The Reactivity of CsPbBr3 Nanocrystals toward Acid/Base Ligands, *ACS Nano*, 2022, **16**, 1444-1455.
33. Y. Tan, Y. Zou, L. Wu, Q. Huang, D. Yang, M. Chen, M. Ban, C. Wu, T. Wu, S. Bai, T. Song, Q. Zhang and B. Sun, Highly Luminescent and Stable Perovskite Nanocrystals with Octylphosphonic Acid as a Ligand for Efficient Light-Emitting Diodes, *ACS Applied Materials & Interfaces*, 2018, **10**, 3784-3792.
34. B. Zhang, L. Goldoni, C. Lambruschini, L. Moni, M. Imran, A. Pianetti, V. Pinchetti, S. Brovelli, L. De Trizio and L. Manna, Stable and Size Tunable CsPbBr3 Nanocrystals Synthesized with Oleylphosphonic Acid, *Nano Letters*, 2020, **20**, 8847-8853.
35. Q. A. Akkerman, V. D'Innocenzo, S. Accornero, A. Scarpellini, A. Petrozza, M. Prato and L. Manna, Tuning the Optical Properties of Cesium Lead Halide Perovskite Nanocrystals by Anion Exchange Reactions, *Journal of the American Chemical Society*, 2015, **137**, 10276-10281.
36. B. Zhang, L. Goldoni, J. Zito, Z. Dang, G. Almeida, F. Zaccaria, J. de Wit, I. Infante, L. De Trizio and L. Manna, Alkyl Phosphonic Acids Deliver CsPbBr3 Nanocrystals with High Photoluminescence Quantum Yield and Truncated Octahedron Shape, *Chemistry of Materials*, 2019, **31**, 9140-9147.
37. G. Almeida, O. J. Ashton, L. Goldoni, D. Maggioni, U. Petralanda, N. Mishra, Q. A. Akkerman, I. Infante, H. J. Snaith and L. Manna, The Phosphine Oxide Route toward Lead Halide Perovskite Nanocrystals, *Journal of the American Chemical Society*, 2018, **140**, 14878-14886.
38. Y. Shynkarenko, M. I. Bodnarchuk, C. Bernasconi, Y. Berezovska, V. Verteletskyi, S. T. Ochsenbein and M. V. Kovalenko, Direct Synthesis of Quaternary Alkylammonium-Capped Perovskite Nanocrystals for Efficient Blue and Green Light-Emitting Diodes, *ACS Energy Letters*, 2019, **4**, 2703-2711.
39. S. Gutiérrez Álvarez, W. Lin, M. Abdellah, J. Meng, K. Žídek, T. Pullerits and K. Zheng, Charge Carrier Diffusion Dynamics in Multisized Quaternary Alkylammonium-Capped CsPbBr3 Perovskite Nanocrystal Solids, *ACS Applied Materials & Interfaces*, 2021, **13**, 44742-44750.
40. Y. Wu, C. Wei, X. Li, Y. Li, S. Qiu, W. Shen, B. Cai, Z. Sun, D. Yang, Z. Deng and H. Zeng, In Situ Passivation of PbBr64–Octahedra toward Blue Luminescent CsPbBr3 Nanoplatelets with Near 100% Absolute Quantum Yield, *ACS Energy Letters*, 2018, **3**, 2030-2037.
41. J.-R. Wen, F. A. Rodríguez Ortiz, A. Champ and M. T. Sheldon, Kinetic Control for Continuously Tunable Lattice Parameters, Size, and Composition during CsPbX3 (X = Cl, Br, I) Nanorod Synthesis, *ACS Nano*, 2022, **16**, 8318-8328.
42. J. Maes, L. Balcaen, E. Drijvers, Q. Zhao, J. De Roo, A. Vantomme, F. Vanhaecke, P. Geiregat and Z. Hens, Light Absorption Coefficient of CsPbBr3 Perovskite Nanocrystals, *The Journal of Physical Chemistry Letters*, 2018, **9**, 3093-3097.
43. Y. Kuang, C. Zhu, W. He, X. Wang, Y. He, X. Ran and L. Guo, Regulated Exciton Dynamics and Optical Properties of Single Perovskite CsPbBr3 Quantum Dots by Diluting Surface Ligands, *The Journal of Physical Chemistry C*, 2020, **124**, 23905-23912.
44. Y. H. Kim, C. Wolf, Y. T. Kim, H. Cho, W. Kwon, S. Do, A. Sadhanala, C. G. Park, S. W. Rhee, S. H. Im, R. H. Friend and T. W. Lee, Highly Efficient Light-Emitting Diodes of Colloidal Metal-Halide Perovskite Nanocrystals beyond Quantum Size, *ACS Nano*, 2017, **11**, 6586-6593.
45. M. C. Brennan, J. E. Herr, T. S. Nguyen-Beck, J. Zinna, S. Draguta, S. Rouvimov, J. Parkhill and M. Kuno, Origin of the Size-Dependent Stokes Shift in CsPbBr3 Perovskite Nanocrystals, *Journal of the American Chemical Society*, 2017, **139**, 12201-12208.
46. J. C. Dahl, X. Wang, X. Huang, E. M. Chan and A. P. Alivisatos, Elucidating the Weakly Reversible Cs–Pb–Br Perovskite Nanocrystal Reaction Network with High-Throughput Maps and Transformations, *Journal of the American Chemical Society*, 2020, **142**, 11915-11926.
47. A. Stelmakh, M. Aebli, A. Baumketner and M. V. Kovalenko, On the Mechanism of Alkylammonium Ligands Binding to

the Surface of CsPbBr3 Nanocrystals, *Chemistry of Materials*, 2021, **33**, 5962-5973.
48. A. Dutta, S. K. Dutta, S. Das Adhikari and N. Pradhan, Tuning the Size of CsPbBr3 Nanocrystals: All at One Constant Temperature, *ACS Energy Letters*, 2018, **3**, 329-334.
49. Y. Huang, W. Luan, M. Liu and L. Turyanska, DDAB-assisted synthesis of iodine-rich CsPbI3 perovskite nanocrystals with improved stability in multiple environments, *Journal of Materials Chemistry C*, 2020, **8**, 2381-2387.
50. R. Grisorio, D. Conelli, E. Fanizza, M. Striccoli, D. Altamura, C. Giannini, I. Allegretta, R. Terzano, M. Irimia-Vladu, N. Margiotta and G. P. Suranna, Size-tunable and stable cesium lead-bromide perovskite nanocubes with near-unity photoluminescence quantum yield, *Nanoscale Advances*, 2021, **3**, 3918-3928.
51. R. Grisorio, E. Fanizza, I. Allegretta, D. Altamura, M. Striccoli, R. Terzano, C. Giannini, V. Vergaro, G. Ciccarella, N. Margiotta and G. P. Suranna, Insights into the role of the lead/surfactant ratio in the formation and passivation of cesium lead bromide perovskite nanocrystals, *Nanoscale*, 2020, **12**, 623-637.
52. R. Grisorio, D. Conelli, R. Giannelli, E. Fanizza, M. Striccoli, D. Altamura, C. Giannini, I. Allegretta, R. Terzano and G. P. Suranna, A new route for the shape differentiation of cesium lead bromide perovskite nanocrystals with near-unity photoluminescence quantum yield, *Nanoscale*, 2020, **12**, 17053-17063.
53. S. R. Smock, Y. Chen, A. J. Rossini and R. L. Brutchey, The Surface Chemistry and Structure of Colloidal Lead Halide Perovskite Nanocrystals, *Accounts of Chemical Research*, 2021, **54**, 707-718.
54. D. P. Nenon, K. Pressler, J. Kang, B. A. Koscher, J. H. Olshansky, W. T. Osowiecki, M. A. Koc, L.-W. Wang and A. P. Alivisatos, Design Principles for Trap-Free CsPbX3 Nanocrystals: Enumerating and Eliminating Surface Halide Vacancies with Softer Lewis Bases, *Journal of the American Chemical Society*, 2018, **140**, 17760-17772.
55. V. K. Ravi, P. K. Santra, N. Joshi, J. Chugh, S. K. Singh, H. Rensmo, P. Ghosh and A. Nag, Origin of the Substitution Mechanism for the Binding of Organic Ligands on the Surface of CsPbBr3 Perovskite Nanocubes, *The Journal of Physical Chemistry Letters*, 2017, **8**, 4988-4994.
56. M. Zhang, Z. Zheng, Q. Fu, Z. Chen, J. He, S. Zhang, L. Yan, Y. Hu and W. Luo, Growth and characterization of all-inorganic lead halide perovskite semiconductor CsPbBr3 single crystals, *CrystEngComm*, 2017, **19**, 6797-6803.
57. Q. Zhang, B. Wang, W. Zheng, L. Kong, Q. Wan, C. Zhang, Z. Li, X. Cao, M. Liu and L. Li, Ceramic-like stable CsPbBr3 nanocrystals encapsulated in silica derived from molecular sieve templates, *Nature Communications*, 2020, **11**, 31.
58. S. Mourdikoudis, M. Menelaou, N. Fiuza-Maneiro, G. Zheng, S. Wei, J. Pérez-Juste, L. Polavarapu and Z. Sofer, Oleic acid/oleylamine ligand pair: a versatile combination in the synthesis of colloidal nanoparticles, *Nanoscale Horizons*, 2022, **7**, 941-1015.
59. N. V. Jadhav, A. I. Prasad, A. Kumar, R. Mishra, S. Dhara, K. R. Babu, C. L. Prajapat, N. L. Misra, R. S. Ningthoujam, B. N. Pandey and R. K. Vatsa, Synthesis of oleic acid functionalized Fe3O4 magnetic nanoparticles and studying their interaction with tumor cells for potential hyperthermia applications, *Colloids and Surfaces B: Biointerfaces*, 2013, **108**, 158-168.
60. F. Lan, J. Bai and H. Wang, The preparation of oleylamine modified micro-size sphere silver particles and its application in crystalline silicon solar cells, *RSC Advances*, 2018, **8**, 16866-16872.
61. A. A. M. Brown, T. J. N. Hooper, S. A. Veldhuis, X. Y. Chin, A. Bruno, P. Vashishtha, J. N. Tey, L. Jiang, B. Damodaran, S. H. Pu, S. G. Mhaisalkar and N. Mathews, Self-assembly of a robust hydrogen-bonded octylphosphonate network on cesium lead bromide perovskite nanocrystals for light-emitting diodes, *Nanoscale*, 2019, **11**, 12370-12380.
62. R. Grisorio, M. E. Di Clemente, E. Fanizza, I. Allegretta, D. Altamura, M. Striccoli, R. Terzano, C. Giannini, M. Irimia-Vladu and G. P. Suranna, Exploring the surface chemistry of cesium lead halide perovskite nanocrystals, *Nanoscale*, 2019, **11**, 986-999.
63. J. De Roo, N. Yazdani, E. Drijvers, A. Lauria, J. Maes, J. S. Owen, I. Van Driessche, M. Niederberger, V. Wood, J. C. Martins, I. Infante and Z. Hens, Probing Solvent–Ligand Interactions in Colloidal Nanocrystals by the NMR Line Broadening, *Chemistry of Materials*, 2018, **30**, 5485-5492.
64. J. Pan, S. P. Sarmah, B. Murali, I. Dursun, W. Peng, M. R. Parida, J. Liu, L. Sinatra, N. Alyami, C. Zhao, E. Alarousu, T. K. Ng, B. S. Ooi, O. M. Bakr and O. F. Mohammed, Air-Stable Surface-Passivated Perovskite Quantum Dots for Ultra-Robust, Single- and Two-Photon-Induced Amplified Spontaneous Emission, *The Journal of Physical Chemistry Letters*, 2015, **6**, 5027-5033.
65. J. De Roo, M. Ibáñez, P. Geiregat, G. Nedelcu, W. Walravens, J. Maes, J. C. Martins, I. Van Driessche, M. V. Kovalenko and Z. Hens, Highly Dynamic Ligand Binding and Light Absorption Coefficient of Cesium Lead Bromide Perovskite Nanocrystals, *ACS Nano*, 2016, **10**, 2071-2081.
66. G. Jones, II, W. R. Jackson, C. Y. Choi and W. R. Bergmark, Solvent effects on emission yield and lifetime for coumarin laser dyes. Requirements for a rotatory decay mechanism, *The Journal of Physical Chemistry*, 1985, **89**, 294-300.